Research Square

Preprints are preliminary reports that have not undergone peer review.
They should not be considered conclusive, used to inform clinical practice,
or referenced by the media as validated information.

AnnoTools: A modular object-based framework for multiplexed immunofluorescence image analysis

Alec K. McKendell
Icahn School of Medicine at Mount Sinai
Ethan Wang
Icahn School of Medicine at Mount Sinai
Dan E. Meyer
GE HealthCare Technology & Innovation Center
Parag Mallick
Stanford University School of Medicine
Patrick R. Hof
Icahn School of Medicine at Mount Sinai
Merina T. Varghese
merina.varghese@uri.edu

University of Rhode Island

Article

Keywords: Spatial biology, object-based hierarchy, proximity analysis, marker overlap, marker coverage, normalization

Posted Date: November 19th, 2026

DOI: https://doi.org/10.21203/rs.3.rs-11570169/v1

License: This work is licensed under a Creative Commons Attribution 4.0 International License.
Read Full License

Additional Declarations: No competing interests reported.

Title: *AnnoTools*: A modular object-based framework for multiplexed immunofluorescence image analysis

Author information
Alec K. McKendell[1], Ethan Wang[1], Dan E. Meyer[2], Parag Mallick[3], Patrick R. Hof[1,4], Merina T. Varghese[5*]

Affiliations
[1] Nash Family Department of Neuroscience and Friedman Brain Institute, Icahn School of Medicine at Mount Sinai, New York, NY 10019, USA
[2] GE HealthCare Technology & Innovation Center, Niskayuna, NY 12309, USA
[3] Canary Center at Stanford for Cancer Early Detection, Department of Radiology, Stanford University School of Medicine, Palo Alto, CA 94304, USA
[4] Ronald M. Loeb Center for Alzheimer's Disease and Alzheimer's Disease Research Center, Icahn School of Medicine at Mount Sinai, New York, NY 10029, USA
[5] George & Anne Ryan Institute for Neuroscience, Department of Biomedical & Pharmaceutical Sciences, University of Rhode Island, Kingston, RI 02881, USA

*** Corresponding Author:**
Dr. Merina T. Varghese, PhD
Assistant Professor
George & Anne Ryan Institute for Neuroscience
Department of Biomedical & Pharmaceutical Sciences
University of Rhode Island
130 Flagg Road
SSRC 006
Kingston, RI 02881, USA
Phone: 401.874.2359
Email: merina.varghese@uri.edu

Keywords: Spatial biology, object-based hierarchy, proximity analysis, marker overlap, marker coverage, normalization

Abstract

Highly multiplexed immunofluorescence imaging (MxIF) enables simultaneous visualization of dozens of molecular markers while preserving tissue architecture and spatial relationships. However, translating spatial relationships observed in biological images into reproducible quantitative measurements often requires segmented objects to be further refined, organized, spatially related, and quantified while maintaining their biological context. Here, we present *AnnoTools*, a modular extension for the open-source image analysis software QuPath that facilitates these post-segmentation stages of object-based image analysis. *AnnoTools* provides interoperable tools for object refinement, geometric manipulation, multi-user object classification, spatial overlap analysis, preservation of hierarchical relationships, and data export. Individual modules can be incorporated into existing workflows or combined according to the biological question being addressed, while remaining agnostic to the method used to generate the underlying objects. Using MxIF images of postmortem human brain tissue, we demonstrate this framework through the established spatial association between astrocytes and cerebral vasculature, translating a visually apparent biological relationship into measurements of astrocyte coverage as a function of distance from blood vessels, which we validate against a negative control. Although demonstrated using MxIF images of postmortem brains, *AnnoTools* provides a flexible framework for translating spatial relationships observed across biological imaging applications into reproducible, inspectable object-based measurements.

Introduction

Spatial transcriptomic, metabolomic, and proteomic imaging have greatly expanded our ability to characterize the molecular composition and organization of biological tissues. As these datasets become increasingly information-rich, extracting biologically meaningful spatial measurements has become an important challenge. Researchers often begin with relatively intuitive observations in an image, for example, whether a cellular marker appears associated with a blood vessel or pathological feature, or whether that association changes with distance. Although segmentation can identify the biological structures involved, it does not necessarily provide the measurements needed to answer these questions. Segmented objects must often be further refined, organized, spatially related to one another, and quantified while maintaining their biological context.

Numerous software platforms address different components of this process. General-purpose image analysis software such as ImageJ/Fiji, CellProfiler, and ilastik provide flexible approaches for image processing, segmentation, and feature extraction, while commercial platforms including HALO (Indica Labs) and AIVIA (Leica Microsystems) provide integrated image analysis capabilities[1-6]. Specialized frameworks such as Squidpy provide powerful methods for downstream spatial analysis[7]. However, these platforms differ substantially in their intended roles and analytical capabilities, and complex workflows may require movement between software environments or custom scripting to connect individual analytical stages (**Supplementary Table S1**). In particular, there remains a need for accessible tools that allow researchers to interact with segmented biological objects after segmentation: refining their properties, manipulating their geometry, preserving relationships between objects, visually

inspecting spatial measurements, and combining these operations according to the biological question being addressed.

QuPath provides a useful foundation for such object-based workflows by combining whole-slide image visualization, annotation, scripting, and project management within an extensible open-source platform[8]. However, implementing a cohesive workflow for post-segmentation object refinement, preservation of hierarchical relationships, geometric manipulation, spatial analysis, and standardized data export still requires additional tooling. Here, we present *AnnoTools*, a modular QuPath extension designed to bridge these downstream stages of image analysis. Rather than introducing another segmentation framework, *AnnoTools* operates on user-defined biological objects after segmentation and provides interoperable tools for object refinement, classification, organization, and exchange. Individual modules can be incorporated independently into existing workflows or combined into an end-to-end analysis depending on the biological question.

AnnoTools was designed around three principles: modularity, extensibility, and flexibility. Once biological structures have been segmented, the same objects can serve as the basis for multiple analyses without repeating earlier image-processing steps. Because the framework operates on QuPath annotation objects rather than requiring a specific segmentation method, any iteration of objects that can either be generated in or imported into QuPath can be incorporated into the workflow. Analyses can then branch into various modules according to the question being asked. Examples include adding morphological or intensity measurements to an object, generating defined spatial regions around it, determining its overlap with another marker, or incorporating expert classifications while retaining object identities, metadata, and hierarchical relationships. Therefore, the biological question determines which analytical modules are used rather than requiring every dataset to pass through a fixed pipeline.

To demonstrate this approach, we applied *AnnoTools* to MxIF images of postmortem human brain tissue and used the spatial relationship between astrocytes and blood vessels as an example for application of the various modules. Astrocytic processes closely associate with the cerebral vasculature, providing an intuitive biological relationship that can be observed in immunofluorescence images and quantified spatially[9,10]. Using segmented astrocytic and vascular markers, we demonstrate how *AnnoTools* can transform this observation into measurements of astrocyte coverage on and at defined distances from blood vessels while preserving the underlying biological objects throughout the analysis. Additional examples demonstrate how the same framework supports object exchange, measurement, geometric manipulation, and manual classification. Although demonstrated using MxIF images of human brain tissue, *AnnoTools* is intended as a general framework for researchers seeking to translate visually apparent relationships in biological images into reproducible object-based measurements.

Results

From a biological observation to an object-based spatial measurement

To demonstrate the application of *AnnoTools*, we used Cell DIVE MxIF images generated from 4-µm-thick postmortem human brain tissue sections from the neocortex of cognitively healthy controls and those with Alzheimer's disease (AD) and exported as stitched OME-TIFF files for visualization and analysis in QuPath[11,12]. The multiplexed panel contained markers representing cell types, cell states, cellular features, tissue architecture, and AD neuropathology including amyloid-β (Aβ) plaques and neurofibrillary tangles comprised of hyperphosphorylated tau (pTau). Within these images, biological structures were represented as QuPath annotation objects, which provide user-modifiable geometries with stored information such as name, class, metadata, measurements, and hierarchical relationships. Although QuPath also supports detection objects with automatically calculated intensity and shape measurements, annotations provide greater flexibility for post-segmentation modification and therefore serve as the primary object type used throughout the *AnnoTools* workflow described here (**Supplementary Fig. S1**).

A central goal of *AnnoTools* is to allow researchers to translate spatial relationships observed in biological images into quantitative measurements. We illustrate this process using the relationship between astrocytes and cerebral blood vessels (**Fig. 1**). Astrocytic processes closely associate with the vasculature, making their spatial distribution relative to blood vessels an intuitive example of a relationship that can be visually identified in immunofluorescence images but requires additional analytical steps to quantify. In our MxIF images, astrocytes were represented by segmented aldehyde dehydrogenase 1 family member L1 (ALDH1L1) signal and vasculature by segmented collagen IV. Rather than treating these segmentations as the endpoint of the analysis, they serve as biological objects from which the spatial relationship between the two structures can be measured.

The resulting analysis can be framed as a sequence of biological questions and object-based operations (**Fig. 1**). First, segmentation identifies the astrocytic and vascular structures visible in the image (**Supplementary Fig. S1**). Vascular objects can then be used as spatial reference features around which *AnnoTools* generates user-defined concentric regions of interest, allowing astrocyte signal to be examined at increasing distances from the blood vessel (**Fig. 2**). *AnnoTools* subsequently identifies the spatial overlap between the astrocytic segmentation and the vascular object or its surrounding regions, generating explicit annotations at their overlap that can be visually inspected and quantified (**Fig. 3**). These measurements can then be exported and normalized to account for variation in total segmented astrocyte area (**Fig. 4**). Together, these operations transform the initial observation that astrocytic processes appear associated with blood vessels into a reproducible measurement of astrocyte coverage as a function of distance from the vasculature.

Importantly, this sequence represents one possible combination of *AnnoTools* modules rather than a fixed linear pipeline. The same segmented objects can be used independently for other analyses. The astrocyte-vascular example therefore provides an end-to-end

demonstration of the framework, while the following sections describe the individual modules that can be selected and combined according to the biological questions being addressed.

Preserving biological context during object exchange:

Object-based spatial analyses often depend on maintaining relationships between biological structures throughout the analytical workflow. QuPath represents these relationships through an object hierarchy in which annotations can contain nested child objects, preserving context such as the cortical layer containing a blood vessel or the association between a biological feature and biologically relevant spatial regions associated with it (**Fig. 5a,b,d,e**). As analyses become more complex, particularly with MxIF images, a single image may accumulate many classes of segmented and derived objects. Keeping all these objects within an active project can make the workflow increasingly difficult to manage and increase computational demand. It can therefore be useful to store related object sets externally and reintroduce them only when needed. For example, the astrocyte-vascular workflow described here can include separate astrocyte and vascular segmentations, concentric regions surrounding the vascular objects, and overlap annotations between the astrocytic signal and each of these regions. Exporting and storing these objects together preserves a completed stage of the analysis that can later be restored and used as the starting point for additional downstream analyses.

Preserving the relationships among these objects during storage and exchange is essential if they are to remain reusable. Although QuPath project data files preserve the complete object hierarchy, they are less suited to selectively storing and retrieving specific groups of annotations. Individual annotations can instead be exported as GeoJSON files, but this process can flatten the object hierarchy, causing parent-child relationships to be lost upon reimport. QuPath allows for these relationships to be constructed but relies on the intended child object to be spatially contained within the parent, which fails when objects share boundaries or are not completely enclosed (**Fig. 5c,f**). Consequently, externally storing a related set of segmented and derived objects requires a mechanism for restoring not only their geometries and classifications, but also the relationships that allow the collection to function as a coherent starting point for subsequent analyses.

To address this limitation, *AnnoTools* provides an "*Export or Import*" function that allows individual annotations or related object sets to be stored externally and subsequently restored while preserving their hierarchical relationships. During export, identifiers linking each child annotation to its parent are stored within the annotation metadata and retained in the resulting GeoJSON file. Upon reimport, *AnnoTools* uses this information to reconstruct the original hierarchy, including when parent annotations already exist in the destination image. Related object classes can therefore be stored together as reusable analytical sets, allowing completed stages of an analysis to serve as starting points for additional *AnnoTools* modules without requiring all intermediate objects to remain in the active project. This also facilitates exchange between projects or users while retaining the spatial and biological context required for downstream analysis.

Refining / Adding information to objects:

Building upon QuPath's flexible annotation framework, *AnnoTools* provides tools for object refinement, spatial transformation, and manual annotation classification. Although segmentation identifies biological structures of interest, additional refinement is often required before biologically meaningful measurements can be extracted. This may include adding measurements to segmented objects, modifying their geometry to define new spatial regions of interest, or incorporating independent users' classifications. The following modules support these operations while preserving object relationships within the QuPath hierarchy.

a) Adding shape and intensity measurements to annotations. Annotation objects in QuPath are designed to be user-modifiable and therefore provide greater flexibility for post-segmentation refinement than detection objects but contain a more limited set of measurements by default. QuPath provides built-in functions for calculating additional intensity and shape measurements for annotations. To simplify and standardize their application across large projects, *AnnoTools* includes an "*Add measurements"* function that selectively applies user-defined QuPath measurements to specified annotation classes across an entire project. Thus, the function uses QuPath's existing measurement calculations rather than introducing independent measurement algorithms. For example, we added circularity and mean pathological Aβ-channel intensity measurements to blood vessel annotations to identify approximate vessel cross-sections (circularity ≥0.5) and quantify vascular Aβ respectively (**Fig. 6**).

b) Adding concentric rings to annotations. Many biological questions depend on quantifying how a marker or cellular feature changes with distance from a biological structure of interest. For example, the close association between astrocytic processes and blood vessels raises the question of how astrocyte coverage changes with increasing distance from the vasculature. Several approaches have been developed to quantify spatial proximity, including nearest-neighbor measurements, radial profiling, and spatial point-pattern analyses such as Ripley's K function[7,13-15]. However, these approaches often represent one or both biological structures as points or summarize their spatial relationship without generating explicit regions that preserve the geometry of the original object. For analyses in which the shape of the biological feature is itself important, defining distance directly from the boundary of a segmented object provides an alternative way to quantify its surrounding microenvironment.

AnnoTools therefore includes a "*Make rings*" function that generates user-defined concentric regions around annotation objects while preserving their relationship to the originating object. Although QuPath provides a native annotation expansion tool, multiple expansions can introduce geometric issues and are difficult to track because they retain the source class and are not hierarchically linked to their originating annotation. *Make rings* builds upon QuPath's existing geometric operations to generate successive expansions and subtract inner regions, producing discrete concentric annotations at user-defined distances (**Fig. 2**). A descriptive class is assigned to each ring based on the source annotation and expansion distance and can be nested beneath the originating object within the QuPath hierarchy. The function can be applied to individual annotations or multi-object masks while preventing outer distance intervals from overlapping corresponding inner regions. These derived annotations can

subsequently serve as spatial regions for downstream measurements, allowing marker coverage or other properties to be quantified as a function of distance from the original biological structure.

c) Adding subclassifications to annotations. Automated segmentation does not always provide sufficient information to distinguish biologically meaningful subclasses of objects. Variable staining intensity, heterogeneous morphology, or limited training data can make some classifications difficult to automate reliably, particularly in human postmortem brains. For example, after segmenting neuronal cell bodies in our MxIF images, we sought to determine whether individual neurons contained pTau, representing NFTs. Variation in pTau signal intensity and morphology made a simple intensity threshold unreliable, while the limited size of our pilot dataset restricted the feasibility of training a robust machine-learning classifier. Expert-guided classification therefore remained useful for assigning this additional information to the segmented neuronal objects.

AnnoTools provides a "*Manual classification*" function that allows multiple users to efficiently review and subclassify large numbers of annotations while retaining those classifications within the object metadata (**Fig. 7**). Annotations are presented in spatially organized groups as the user progresses through the image, with controls for displaying relevant image channels, adjusting channel brightness, and defining subclassification states. Individual objects can be classified directly within the image viewer or examined at higher magnification when additional context is needed. The resulting classification and reviewer identity are stored with each annotation, allowing the same objects to be independently evaluated by multiple users. Classified objects can subsequently be exchanged using the "*Export or Import*" function, allowing multiple users to independently classify the same objects and a reviewer to resolve differences in classification.

Coverage analysis:

Many biological questions require quantifying the spatial association between a marker of interest and a biological feature, such as the extent to which astrocytic processes are associated with blood vessels. In two-dimensional tissue sections, these relationships are not always adequately represented by object counts or distance measurements between two points, particularly for highly ramified cell types whose processes extend across irregularly shaped structures. For these relationships, the area of spatial overlap between segmented objects can provide a more direct measure of their association.

AnnoTools includes a "*Find colocalizations*" function that generates new annotation objects representing the spatial intersection between two existing annotation classes. Rather than returning overlap solely as a numerical measurement, the intersecting geometry is retained as an explicit annotation that can be visually inspected, quality controlled, and used for subsequent coverage measurements (**Fig. 3**). One annotation class is designated as the biological feature and the second as the marker of interest. For example, the intersection between collagen IV-positive vasculature and an astrocytic marker generates annotations representing the astrocyte signal overlapping each vascular object. The same operation can be

applied to the concentric regions generated using *Make rings*, allowing astrocyte coverage to be measured at defined distances from the vessel.

The resulting overlap annotations are assigned descriptive classes reflecting the contributing objects and can be nested beneath the corresponding feature annotation within the QuPath hierarchy. This preserves the relationship between each overlap measurement and the biological structure or spatial region from which it was derived, while allowing the overlap objects to be independently visualized, filtered, measured, and exported.

Data export:

To support downstream statistical analysis and visualization, *AnnoTools* includes a customizable "*Save data*" function for project-wide data export. Users can select annotation classes together with associated measurements and metadata for export across all images in a project, allowing the resulting dataset to be tailored to the biological question being addressed. Because object identities, classifications, measurements, and hierarchical information are retained throughout the *AnnoTools* workflow, these properties can be incorporated into the exported dataset for subsequent analysis.

Coverage normalization:

Raw coverage measurements quantify the proportion of a biological feature that overlaps with a marker of interest, but their interpretation depends on the overall abundance of that marker within the tissue. For example, an image containing more segmented astrocyte signal may exhibit greater astrocyte coverage of blood vessels simply because astrocytic processes occupy a larger proportion of the tissue, rather than because they are more specifically associated with the vasculature. Differences in segmented marker area can arise from biological variation in highly ramified cell populations as well as technical factors such as staining intensity, antibody performance, and imaging conditions.

To account for this variability, we normalized the coverage of a feature by a marker to the overall coverage of that marker within the surrounding tissue. The normalized coverage of a marker on a feature (NC_{MF}) was calculated as

$$NC_{MF} = (A_{MF} / A_F) \ / \ (A_M / A_T)$$

where A_{MF} represents the area of overlap between the marker and feature, A_F represents the total area of the feature, A_M represents the total segmented area of the marker, and A_T represents the analyzed tissue area. The first term (A_{MF}/A_F) represents the fraction of the feature covered by the marker, whereas the second (A_M/A_T) represents the fraction of the surrounding tissue occupied by that marker. NC_{MF} therefore expresses feature coverage relative to the marker's overall tissue coverage, providing a measure of whether the marker is preferentially associated with the feature compared with its background distribution. Similar

normalization strategies have been used to address the challenges associated with quantifying ramified glial morphology in immunofluorescence[16,17].

For the astrocyte-vascular analysis, the astrocytic signal represents the marker and vascular signal represents the feature. The normalized coverage of astrocytes on vasculature (NC_{AV}) was therefore calculated as

$$NC_{AV} = (A_{AV} / A_V) / (A_A / A_T)$$

where A_{AV} represents the area of overlap between astrocyte and vascular segmentations, A_V represents the total segmented vascular area, A_A represents the total segmented astrocyte area, and A_T represents the analyzed tissue area. An NC_{AV} value of 1 indicates that astrocyte coverage of vasculature is equivalent to the overall astrocyte coverage of the tissue, whereas values greater than 1 indicate preferential localization of astrocytic signal to vasculature (**Fig. 4**). The same normalization can be applied to the distance-defined rings generated around vessels, allowing astrocyte enrichment to be compared as a function of distance from the vascular surface.

Normalization was performed in R[18] using data exported from QuPath, separating object generation and spatial measurements from downstream statistical analysis and visualization. This normalization is intended for coverage-based measurements of continuous or spatially diffuse signals rather than discrete object counts, for which alternative normalization strategies may be more appropriate.

Validation of spatial analyses:

To evaluate the ability of *AnnoTools* to recover biologically meaningful spatial relationships, we used the established association between astrocytic processes and cerebral vasculature as a positive control. Astrocyte coverage was quantified within segmented blood vessels and concentric regions at increasing distances from the vasculature. As a negative control, the vascular objects were spatially randomized within each image while ensuring they did not overlap and remained fully within the analyzed tissue region, after which the same analysis was repeated using their new locations. Astrocyte coverage was greatest at true vascular locations and decreased with increasing distance, whereas the shuffled vascular objects showed no comparable distance-dependent pattern (**Supplementary Fig. S4**).

Discussion

MxIF has become increasingly useful for studying the spatial organization of cells and pathological features within intact tissue, particularly in diseases such as AD where interactions among glial cells, pathological protein aggregates, vasculature, and vulnerable neuronal populations are closely associated with disease progression[16,19-21]. Importantly, many of these questions are not unique to MxIF. Conventional immunofluorescence studies have similarly

examined whether cellular populations associate with pathological features, whether marker coverage differs across tissue regions, and how cellular responses vary with proximity to structures such as Aβ deposits[17,22-26]. These questions are often visually intuitive but require several analytical steps to quantify. Although segmentation identifies the biological structures involved, those objects may require further refinement, organization, and spatial analysis before an observation can be converted into a quantitative measurement. *AnnoTools* was developed to facilitate this transition by providing an object-based framework in which segmented biological structures can be manipulated, related, and quantified while remaining connected to their original image and biological context.

A central feature of this approach is that the biological objects, rather than a predefined analysis pipeline, form the basis of the workflow. Once generated, the same objects can support multiple analyses without repeating segmentation or earlier processing steps. Measurements and classifications can be added directly to existing objects, new spatial regions can be derived from their geometry, and relationships between objects can be represented through explicit overlap annotations and hierarchical associations. These operations can be performed independently or combined when a biological question requires multiple analytical steps, as demonstrated by the astrocyte-vascular workflow presented here. Because these derived measurements and annotations remain associated with their source objects, users can visually inspect intermediate results and maintain biological context as analysis becomes progressively more complex.

The validation analysis further demonstrated the utility of *AnnoTools* for quantifying biologically meaningful spatial relationships. By recovering the expected enrichment of astrocyte signal at blood vessels while showing no comparable pattern following spatial shuffling of those vascular objects, the workflow demonstrated its ability to distinguish established biological spatial organization from a randomized negative control (**Supplementary Fig. S4**). Importantly, this analysis was intended to demonstrate the analytical capabilities of *AnnoTools* rather than test disease-associated differences in astrocyte biology, which will be investigated in a subsequent study with a larger cohort.

Although automation continues to improve many aspects of image analysis, manual interpretation remains important when biological structures cannot be classified reliably using automated approaches. Variable staining intensity, heterogeneous pathology, and complex cellular morphologies can make this particularly relevant in human postmortem tissues such as the brain. *AnnoTools* incorporates manual classification into the same object-based framework while preserving object identity, metadata, and spatial context. Because these objects can be exchanged between users, multiple reviewers can independently classify the same annotations, allowing agreement to be assessed and disagreements to be resolved while retaining access to the underlying image. This multi-reviewer approach increases the rigor and reproducibility of manual classification while generating curated object sets that may also provide training data for future machine-learning approaches as larger datasets become available.

As with any object-based analysis, the accuracy of downstream measurements depends on the quality of the objects provided to the workflow. *AnnoTools* is intentionally agnostic to

segmentation strategy and can operate on annotations generated using thresholding, machine-learning approaches, manual annotation, or other methods. However, inaccurate or inconsistent segmentation will propagate into subsequent spatial measurements. *AnnoTools* is therefore intended to complement rather than replace dedicated segmentation methods or specialized spatial-analysis platforms. Its primary role is to facilitate the post-segmentation refinement, manipulation, and organization of biological objects and to make these operations accessible within an interactive image-analysis environment. Highly customized analyses may still require QuPath scripting or specialized external software, but individual *AnnoTools* modules can be incorporated into these workflows when appropriate.

The current implementation of *AnnoTools* operates on individual two-dimensional images rather than three-dimensional image stacks. Consequently, measurements of morphology, proximity, and coverage describe relationships within the plane of sectioning and do not capture the complete three-dimensional organization of biological structures. This limitation is particularly relevant for highly ramified cells such as astrocytes, whose processes extend beyond the section plane. Nevertheless, two-dimensional whole-slide imaging remains widely compatible with established histological and multiplexed imaging workflows, making object-based analysis of tissue sections applicable to many biological studies.

As imaging and segmentation technologies continue to evolve, the methods used to identify biological structures will likewise improve. However, the need to organize, refine, relate, and quantify those structures will remain. Because *AnnoTools* operates on segmented biological objects rather than requiring a particular imaging or segmentation strategy, its modules can be incorporated into evolving analytical workflows while maintaining a consistent framework for downstream object-based analysis. Although developed using MxIF images of human brain tissue, the underlying approach is applicable to conventional immunofluorescence and other imaging modalities in which researchers seek to translate spatial relationships observed in an image into quantitative measurements. By keeping these measurements connected to inspectable biological objects, *AnnoTools* provides a flexible framework for moving from biological observation to reproducible spatial analysis.

Materials and Methods

Cohort

The postmortem human specimens used in our analyses were obtained from the Department of Psychiatry, University of Geneva School of Medicine, Geneva, Switzerland and were fully deidentified by the biorepository[25,26]. All donors had provided informed consent and the use of brain specimens for research and teaching is reviewed and controlled by the ethics commission of the University of Geneva School of Medicine. As such, the Institutional Review Board of the Icahn School of Medicine at Mount Sinai determined that these studies are not considered to be research involving human subjects, as defined by the regulations of the Department of Health and Human Services and the Food and Drug Administration (IRB ID:

STUDY-24-00621). All work involving postmortem human brain specimens were performed in accordance with relevant guidelines and regulations.

The specimens represented the dorsolateral prefrontal cortex (DLPFC) and the primary visual cortex (V1) from donors with varying clinical dementia rating (CDR) scores[27,28], Braak stages[29], Thal stages[30], and apolipoprotein-E (*APOE*) genotypes.

MxIF tissue processing and imaging

For each brain region, formalin-fixed, paraffin-embedded tissue microarray cores 4.5 mm in diameter were selected to include all six neocortical layers as well as white matter and sectioned at 5 μm. Two or three technical replicates from cores at different locations of each tissue block were included. The tissue was slide-mounted, subject to deparaffination, antigen retrieval, autofluorescence reduction, and staining with 4′,6-diamidino-2-phenylindole (DAPI) to detect nuclei, imaged for autofluorescence, and then stained with two primary antibodies conjugated with cyanine-based fluorophores as well as DAPI for nuclei and imaged. Antibodies validated for MxIF and relevant to the workflow described in this paper are described in **Supplementary Table S2**. The fluorophores were then inactivated by incubation in an alkaline solution containing hydrogen peroxide, and for each subsequent MxIF cycle, the tissue was re-stained with two new antibodies and DAPI and imaged. Images were taken between cycles to test for signal carryover. Finally, images across rounds are stitched together using the nuclei as reference and the autofluorescence was digitally subtracted. Regions where the nuclei did not align or were missing between cycles of MxIF indicated a fold or damage to the tissue, and quality control maps were made referencing the cycle number and problematic areas which are omitted from final analyses (**Supplementary Fig. S2**). The result is an OME-TIFF file in which each pixel contains a respective intensity value for each marker represented by a channel in QuPath's image viewer[11,12].

Image segmentation

For the workflow presented here, analysis begins by manually annotating the neocortical layers in each image. These layers were delineated using the tissue cytoarchitecture combined with distribution of Hu-antigen D (HUD), a pan-neuronal marker; glial fibrillary acidic protein (GFAP), an astrocytic structural marker; vesicular GABA transporter (VGAT), which labels inhibitory synapses; myelin basic protein (MBP), a marker of myelinated axons that helps define the underlying white matter; and non-phosphorylated neurofilament protein (NPNFP), which is expressed in corticocortical pyramidal neurons located in layers 3 and 5 (antibody specifics can be found in **Supplementary Table S2**). Layer annotations define biologically meaningful regions of interest that represent the laminar organization of the neocortex throughout subsequent analyses (**Supplementary Fig. S2**).

Within these annotated cortical layers, two broad classes of objects were segmented: (i) structural or pathological features that serve as regions of interest (e.g., blood vessels and Aβ),

and (ii) markers representing cell types or cell states (e.g., ALDH1L1 for astrocytes), which often exhibit complex and highly ramified morphologies (**Supplementary Fig. S3**). The workflow described in this paper refines these segmented objects and quantifies their spatial relationships.

Object generation was performed using QuPath's native pixel thresholder for a given marker of interest. QuPath allows for these thresholders to be easily generated, including a preview of the pixels that will be classified as positive when testing a threshold for a given channel. To aid with threshold generation further, the viewer within QuPath will display the intensity in arbitrary units of the channel(s) that are actively enabled, allowing the user to get a sense of the average signal and background/noise values. These thresholders can then be saved locally within the project directory for re-use, application across the entirety of the project, or future modification. Additional parameters can also be edited including the smoothing sigma, spatial prefilter, and minimum size threshold, which are set based on the dynamics of each marker of interest. Finally, when applying the thresholder to the image or project, it can be run specifically within objects of interest.

Because our primary goal was to develop an object-based analysis workflow rather than a segmentation framework, we elected to use QuPath's native pixel thresholders rather than training and/or applying existing machine learning models for segmentation. To generate the most accurate and least biased parameters for each pixel thresholder, the user was blinded to the experimental groups, picking six images at random. After generating and saving pixel thresholders for each marker of interest, they were applied within the neocortical layer annotations across all images in the project. The layer annotations also underwent quality-control, excluding regions with tissue loss or staining artifacts introduced during multiple rounds of MxIF (**Supplementary Fig. S2**). Additionally, by running the thresholders within layer objects, QuPath nests the new segmentation annotations as child objects within the parent neocortical layers, which links the objects together and is recognized in the image object hierarchy. This hierarchy provides the foundation for the downstream *AnnoTools* functions, allowing derived objects to remain associated with their anatomical context throughout the workflow. When exporting data using *AnnoTools*, parent object information is included.

References

1 Schindelin, J. *et al.* Fiji: an open-source platform for biological-image analysis. *Nat Methods* **9**, 676–682 (2012). https://doi.org/10.1038/nmeth.2019

2 Carpenter, A. E. *et al.* CellProfiler: image analysis software for identifying and quantifying cell phenotypes. *Genome Biol* **7**, R100 (2006). https://doi.org/10.1186/gb-2006-7-10-r100

3 McQuin, C. *et al.* CellProfiler 3.0: Next-generation image processing for biology. *PLoS Biol* **16**, e2005970 (2018). https://doi.org/10.1371/journal.pbio.2005970

4 Berg, S. *et al.* ilastik: interactive machine learning for (bio)image analysis. *Nat Methods* **16**, 1226–1232 (2019). https://doi.org/10.1038/s41592-019-0582-9

5 Li, S. J. *et al.* Meshed neuronal mitochondrial networks empowered by AI-powered classifiers and immersive VR reconstruction. *Front Neurosci* **17**, 1059965 (2023). https://doi.org/10.3389/fnins.2023.1059965
6 Chan, N. R. *et al.* Novel HALO(R) image analysis to determine cell phenotype in porous precision-templated scaffolds. *J Biomed Mater Res A* **111**, 1459–1467 (2023). https://doi.org/10.1002/jbm.a.37547
7 Palla, G. *et al.* Squidpy: a scalable framework for spatial omics analysis. *Nat Methods* **19**, 171–178 (2022). https://doi.org/10.1038/s41592-021-01358-2
8 Bankhead, P. *et al.* QuPath: Open source software for digital pathology image analysis. *Sci Rep* **7**, 16878 (2017). https://doi.org/10.1038/s41598-017-17204-5
9 MacVicar, B. A. & Newman, E. A. Astrocyte regulation of blood flow in the brain. *Cold Spring Harb Perspect Biol* **7** (2015). https://doi.org/10.1101/cshperspect.a020388
10 Manu, D. R. *et al.* Astrocyte Involvement in Blood-Brain Barrier Function: A Critical Update Highlighting Novel, Complex, Neurovascular Interactions. *Int J Mol Sci* **24** (2023). https://doi.org/10.3390/ijms242417146
11 Gerdes, M. J. *et al.* Highly multiplexed single-cell analysis of formalin-fixed, paraffin-embedded cancer tissue. *Proc Natl Acad Sci U S A* **110**, 11982–11987 (2013). https://doi.org/10.1073/pnas.1300136110
12 Castro-Mendoza, P. B. *et al.* Proteomic features of gray matter layers and superficial white matter of the rhesus monkey neocortex: comparison of prefrontal area 46 and occipital area 17. *Brain Struct Funct* **229**, 1495–1525 (2024). https://doi.org/10.1007/s00429-024-02819-y
13 Stoltzfus, C. R. *et al.* CytoMAP: A Spatial Analysis Toolbox Reveals Features of Myeloid Cell Organization in Lymphoid Tissues. *Cell Rep* **31**, 107523 (2020). https://doi.org/10.1016/j.celrep.2020.107523
14 Schapiro, D. *et al.* histoCAT: analysis of cell phenotypes and interactions in multiplex image cytometry data. *Nat Methods* **14**, 873–876 (2017). https://doi.org/10.1038/nmeth.4391
15 Behanova, A., Klemm, A. & Wahlby, C. Spatial Statistics for Understanding Tissue Organization. *Front Physiol* **13**, 832417 (2022). https://doi.org/10.3389/fphys.2022.832417
16 Nguyen-Hao, H. T. *et al.* Quantification of Alzheimer disease neuropathology using tissue microarrays. *J Neuropathol Exp Neurol* **84**, 855–869 (2025). https://doi.org/10.1093/jnen/nlaf064
17 Kecheliev, V. *et al.* Aquaporin 4 is differentially increased and dislocated in association with tau and amyloid-beta. *Life Sci* **321**, 121593 (2023). https://doi.org/10.1016/j.lfs.2023.121593
18 R Core Team v. R version 4.1.2 (2021-11-01) (2021).
19 Keene, C. D. *et al.* Luminex-based quantification of Alzheimer's disease neuropathologic change in formalin-fixed post-mortem human brain tissue. *Lab Invest* **99**, 1056–1067 (2019). https://doi.org/10.1038/s41374-018-0165-x
20 Muñoz-Castro, C. *et al.* Cyclic multiplex fluorescent immunohistochemistry and machine learning reveal distinct states of astrocytes and microglia in normal aging and Alzheimer's disease. *J Neuroinflammation* **19**, 30 (2022). https://doi.org/10.1186/s12974-022-02383-4
21 Maskey, D. *et al.* Antibody elution methods for multiplex immunofluorescence of Alzheimer's disease pathology in human post-mortem brain tissue. *Front Neurol* **17**, 1760600 (2026). https://doi.org/10.3389/fneur.2026.1760600
22 Serrano-Pozo, A. *et al.* Differential relationships of reactive astrocytes and microglia to fibrillar amyloid deposits in Alzheimer disease. *J Neuropathol Exp Neurol* **72**, 462–471 (2013). https://doi.org/10.1097/NEN.0b013e3182933788

23 Sanchez-Molina, P. *et al.* Spatial proteomic analysis in human Alzheimer's disease brains enables identification of microenvironment-dependent microglial cell states. *Nat Neurosci* (2026). https://doi.org/10.1038/s41593-026-02267-3
24 Gerrits, E. *et al.* Distinct amyloid-beta and tau-associated microglia profiles in Alzheimer's disease. *Acta Neuropathol* **141**, 681–696 (2021). https://doi.org/10.1007/s00401-021-02263-w
25 Bussière, T. *et al.* Stereologic assessment of the total cortical volume occupied by amyloid deposits and its relationship with cognitive status in aging and Alzheimer's disease. *Neuroscience* **112**, 75–91 (2002). https://doi.org/10.1016/s0306-4522(02)00056-8
26 Bussière, T. *et al.* Progressive degeneration of nonphosphorylated neurofilament protein-enriched pyramidal neurons predicts cognitive impairment in Alzheimer's disease: stereologic analysis of prefrontal cortex area 9. *J Comp Neurol* **463**, 281–302 (2003). https://doi.org/10.1002/cne.10760
27 Hughes, C. P., Berg, L., Danziger, W. L., Coben, L. A. & Martin, R. L. A new clinical scale for the staging of dementia. *Br J Psychiatry* **140**, 566–572 (1982). https://doi.org/10.1192/bjp.140.6.566
28 Morris, J. C. Clinical dementia rating: a reliable and valid diagnostic and staging measure for dementia of the Alzheimer type. *Int Psychogeriatr* **9 Suppl 1**, 173–176; discussion 177–178 (1997). https://doi.org/10.1017/s1041610297004870
29 Braak, H. & Braak, E. Neuropathological stageing of Alzheimer-related changes. *Acta Neuropathol* **82**, 239–259 (1991). https://doi.org/10.1007/BF00308809
30 Thal, D. R., Rüb, U., Orantes, M. & Braak, H. Phases of A beta-deposition in the human brain and its relevance for the development of AD. *Neurology* **58**, 1791–1800 (2002). https://doi.org/10.1212/wnl.58.12.1791

Acknowledgements

We thank Ms. Bridget Wicinski for assistance with specimen preparation and technical support. We thank Ms. Lisa Lowery and Ms. Elizabeth McDonough for generating the MxIF images.

Funding

This work was supported by NIH grants T32 MH087004 and R01 AG078755S1 (to A.K.M.), R56 AG049870, R01 AG059028, and P30 AG066514 (to P.R.H.), and R01 AG078755 (to D.E.M., P.M., P.R.H., M.T.V.).

Author contributions

A.K.M. designed and developed *AnnoTools* with aid in code refinement, debugging, and optimization from ChatGPT (OpenAI) and Claude (Anthropic). All AI-assisted code was reviewed, tested, and validated by the authors prior to use. A.K.M. wrote the first draft and undertook further edits. Feedback and testing of *AnnoTools* was provided by E.W., who also assisted A.K.M. in preparing the figures. D.E.M. and P.M. helped with interpretation of data and substantive revision. D.E.M., P.R.H., M.T.V., and A.K.M. designed the experiments. All authors have read and approved the submitted version.

Competing interests

The authors declare no competing interests.

Data availability

The image data used to demonstrate the software tools developed in this study are owned by GE HealthCare and are not publicly available. The data were used under an agreement governing their use for the current study.

Code availability

Source code for *AnnoTools* is available at Release 0.1.0

Figure legends

Figure 1. Sample end-to-end workflow using *AnnoTools*. Using *AnnoTools* functions in sequence to quantify how astrocytes near blood vessels are localized between a control and AD case. Examples are shown from cortical layer 3 in the DLPFC of an 87-year-old cognitively healthy woman. The workflow is shown both from a **(a-d)** zoomed out and **(e-h)** zoomed in field of view. The panels along the bottom of each column demonstrate how the user-created objects may be organized within the QuPath hierarchy at each respective step of the sample workflow. **(a,e)** MxIF image showing ALDH1L1 (yellow) and collagen IV (magenta) channels. The surrounding layer 3 annotation is shown in the hierarchy. **(b,f)** Respective ALDH1L1 (yellow) and collagen IV (magenta) segmentations, which are nested within the layer 3 annotation in the hierarchy. **(c,g)** Concentric rings at 6 and 16 μm radii (light gray, dark gray, respectively) added to the collagen IV segmentations using the "*Make rings*" function. Within the hierarchy, the rings are nested within the central collagen IV object. **(d,h)** Overlap between the ALDH1L1 segmentations and either the collagen IV segmentations or their concentric rings (white, orange, red respectively), generated using the "*Find colocalization*" function. Within the hierarchy, the overlapping objects are nested within their associated collagen IV object or ring. **(i)** Quantification of ALDH1L1 coverage of collagen IV + rings by ALDH1L1 in the control case described above and an 85-year-old man diagnosed with AD, expressed as the percentage of object area covered by ALDH1L1 (raw coverage) and as the ratio of this percentage to the overall ALDH1L1 coverage of the image (normalized coverage). Error bars represent standard deviation across technical replicates.

Figure 2. Expanding annotations with user-defined geometries. Limitations with QuPath's native object expansion tool are avoided when using the "*Make rings*" function in *AnnoTools*. Examples shown here are from cortical layer 6 **(a-c)** and layer 4 **(d-f)** in the V1 of an 85-year-old man diagnosed with AD. Each image provides an example of objects and their associated expansions (6, 16 μm) when applicable. **(a)** Individual collagen IV segmentations or **(d)** Aβ segmentations as multi-object masks. **(b,e)** QuPath's "Expand annotations" tool allows the user to geometrically subtract the inner object, but attempting to generate more than one concentric ring results in the potential geometric problems introduced by the additional of a second ring, as highlighted in yellow and labeled by each number as follows: (1) expanding twice from the central object results in the second ring encompassing the first; (2) expanding from the first ring results in the second ring encompassing the central object; (3) expansions around nearby objects do not avoid other objects, resulting in overlap. Finally, as demonstrated in the metadata at the bottom, expansions are the same class and are disconnected from the central object. **(c,f)** Using the "*Make rings*" function in *AnnoTools* on the same collagen IV and Aβ segmentations successfully creates concentric rings in all the previously described scenarios (1-3) have descriptive classes based on the class of the central object and the expansion radius and are optionally nested within the central object.

Figure 3. Analyzing overlap between objects. The "*Find colocalization*" function in *AnnoTools* generates objects at the overlapping area between annotation objects. MxIF image of DLPFC

layer 6 from an 83-year-old woman who was diagnosed with AD. **(a)** Collagen IV channel and segmentations are shown in magenta with the respective hierarchy at the bottom. **(b)** ALDH1L1 channel and segmentations are shown in yellow with the respective hierarchy at the bottom. **(c)** The same collagen IV and ALDH1L1 segmentations shown alongside cyan objects generated at their overlap using the "*Find colocalization*" function in *AnnoTools*. The respective hierarchy at the bottom shows the specifics of the novel overlapping object, including a descriptive class ("COLLAGENIV-ALDH1L1) and an optional ability to nest within one of the two overlapping objects.

Figure 4. Normalizing coverage data. An example of the effect of normalization applied to technical replicates varying in ALDH1L1 staining intensity. MxIF images encompass regions of layers 3-5 of the DLPFC from an 85-year-old cognitively healthy man. **(a,e)** ALDH1L1 (yellow) and collagen IV (magenta) channels. **(b,f)** Full ALDH1L1 segmentations (yellow) shown with collagen IV segmentations (magenta). The percentage of the respective image covered by ALDH1L1 is shown at the bottom right. **(c,g)** Collagen IV segmentations (magenta) alongside the area colocalizing with ALDH1L1 segmentations (cyan), generated using the "*Find Colocalization*" function within *AnnoTools*. The percentage of collagen IV segmentations covered by ALDH1L1 segmentations is shown at the bottom right for each image. **(d,h)** Full ALDH1L1 segmentations (yellow) are shown with collagen IV segmentations and their overlap. The equation normalizing the percentage of collagen IV segmentations colocalizing with ALDH1L1 segmentations to the percentage of the image covered with ALDH1L1 segmentations is shown at the bottom right. **(i)** The difference in total ALDH1L1 coverage shown in panels **b** and **f**. **(j)** The difference in ALDH1L1 coverage of collagen IV between panels **c** and **g**. **(k)** The difference in normalized ALDH1L1 coverage of collagen IV, represented as a multiplier of the total image coverage. The red, dotted line at 1x represents the average image coverage of ALDH1L1.

Figure 5. Maintaining hierarchy when saving objects externally. Examples of nested object relationships in QuPath's image viewer and associated hierarchy, which is maintained by exporting and re-importing the objects using the "*Export or Import*" function within *AnnoTools* but lost when using QuPath's native exporting and importing functions. Examples shown here are from cortical layer 5 in the V1 of an 85-year-old man diagnosed with AD. **(a)** An example of a two-level hierarchy consisting of collagen IV segmentations (magenta) within a larger annotated tissue area (white), shown in the hierarchy as **(b)** intact (*AnnoTools*) or **(c)** flattened (native QuPath import). **(d)** A visual demonstration of a three-level hierarchy including Aβ segmentations (yellow), concentric rings (green, blue, purple), and a bounding tissue area annotation (white). **(e)** The relationships between these objects are shown in the hierarchy tab (*AnnoTools*), **(f)** along with a flattened version of the same objects (native QuPath import).

Figure 6. Adding user-defined measurements. Specific channel intensity and morphological measurements can be added to annotation objects using the "*Add measurements*" function in *AnnoTools*. **(a,b)** MxIF image of the V1 layers 3 and 4 from an 85-year-old man who was diagnosed with AD. **(a)** Collagen IV channel and segmentations shown in magenta. **(b)** Aβ channel shown in blue with same collagen IV segmentations. **(c)** Metadata for a selected collagen IV segmentation containing Aβ (yellow outline in panels **a** and **b**), with specific channel intensity (Aβ) and morphology (circularity) measurements that have been added using the "*Add measurements*" function in *AnnoTools*, highlighted in the yellow box.

Figure 7. Adding subclassifications to annotations. The "*Manual classification*" function in *AnnoTools* allows multiple users to manually assign custom classifications to the same annotation objects. Sample of MxIF images from DLPFC layers 4 and 5 from an 83-year-old woman who was diagnosed with AD. Each panel represents a customized field of view using the "*Manual classification*" function within *AnnoTools*. Here, the user is classifying neuronal segmentations (HUD) for whether they contain pathological tau protein (PTAU), called neurofibrillary tangles (NFTs). The square in the middle of the images represents one region of a custom-sized grid (500 μm x 500 μm) that the user interacts with to classify the contained objects. The surrounding filled objects outside of the central square represent those that the user has already classified. **(a)** HUD channel shown in yellow. At the bottom left is a snapshot of the controls for the user-selected channels used to make classifications, showing only the HUD channel turned on. **(b)** PTAU channel shown in blue with the respective channel controls. **(c)** HUD and PTAU channels, with the respective controls showing both channels on and the ability to control the PTAU channel brightness by scrolling on the viewer. **(d)** HUD channel with HUD segmentations as outlines, which are colored based on whether the user classified the objects as false (red) or true (white) for containing PTAU. The surrounding filled objects that have already been classified follow the same color scheme. At the bottom left is a snapshot of the user-defined classification options. **(e)** PTAU channel with the same classified HUD segmentations alongside an example of the classification options when the user's mouse is hovered over a segmentation classified as "true." The cursor is exaggerated in size for visibility. **(f)** The classified HUD segmentations with an example of the metadata entries for a single object classified by two different users. Note the key includes the name of the tool ("AT-manual"), the role of the user ("classifier" vs. "reviewer"), the username (e.g. "User1"), and the classification category ("NFT").

Figure 1

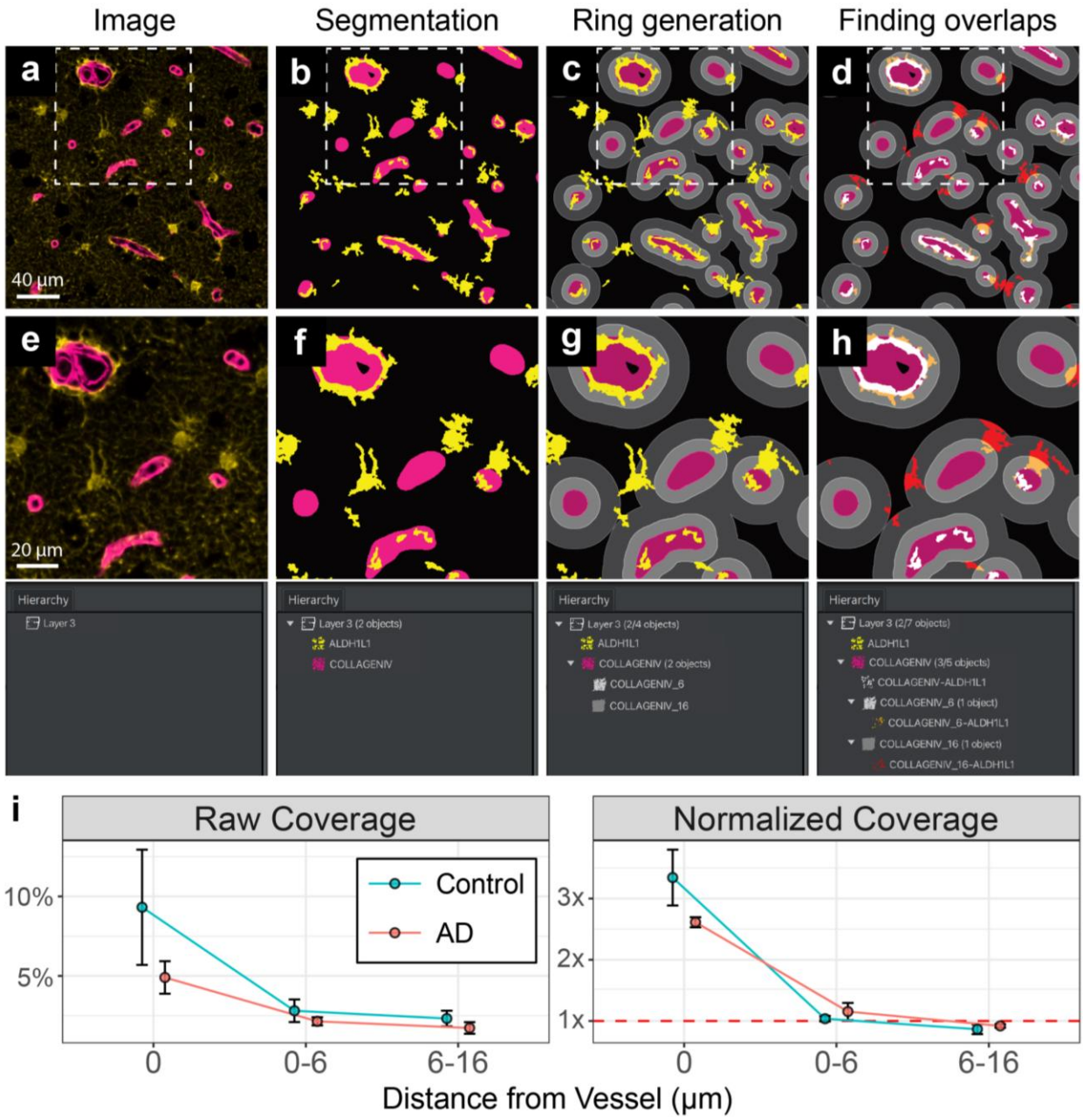

Image
Segmentation
Ring generation
Finding overlaps
a
b
c
d
40 µm
e
f
g
h
20 µm
Hierarchy
Layer 3
Layer 3 (2 objects)
ALDH1L1
COLLAGENIV
Layer 3 (2/4 objects)
COLLAGENIV (2 objects)
COLLAGENIV_6
COLLAGENIV_16
Layer 3 (2/7 objects)
COLLAGENIV (3/5 objects)
COLLAGENIV-ALDH1L1
COLLAGENIV_6 (1 object)
COLLAGENIV_6-ALDH1L1
COLLAGENIV_16 (1 object)
COLLAGENIV_16-ALDH1L1
i
Raw Coverage
Normalized Coverage
Control
AD
10%
5%
3x
2x
1x
0
0-6
6-16
Distance from Vessel (µm)

Figure 2

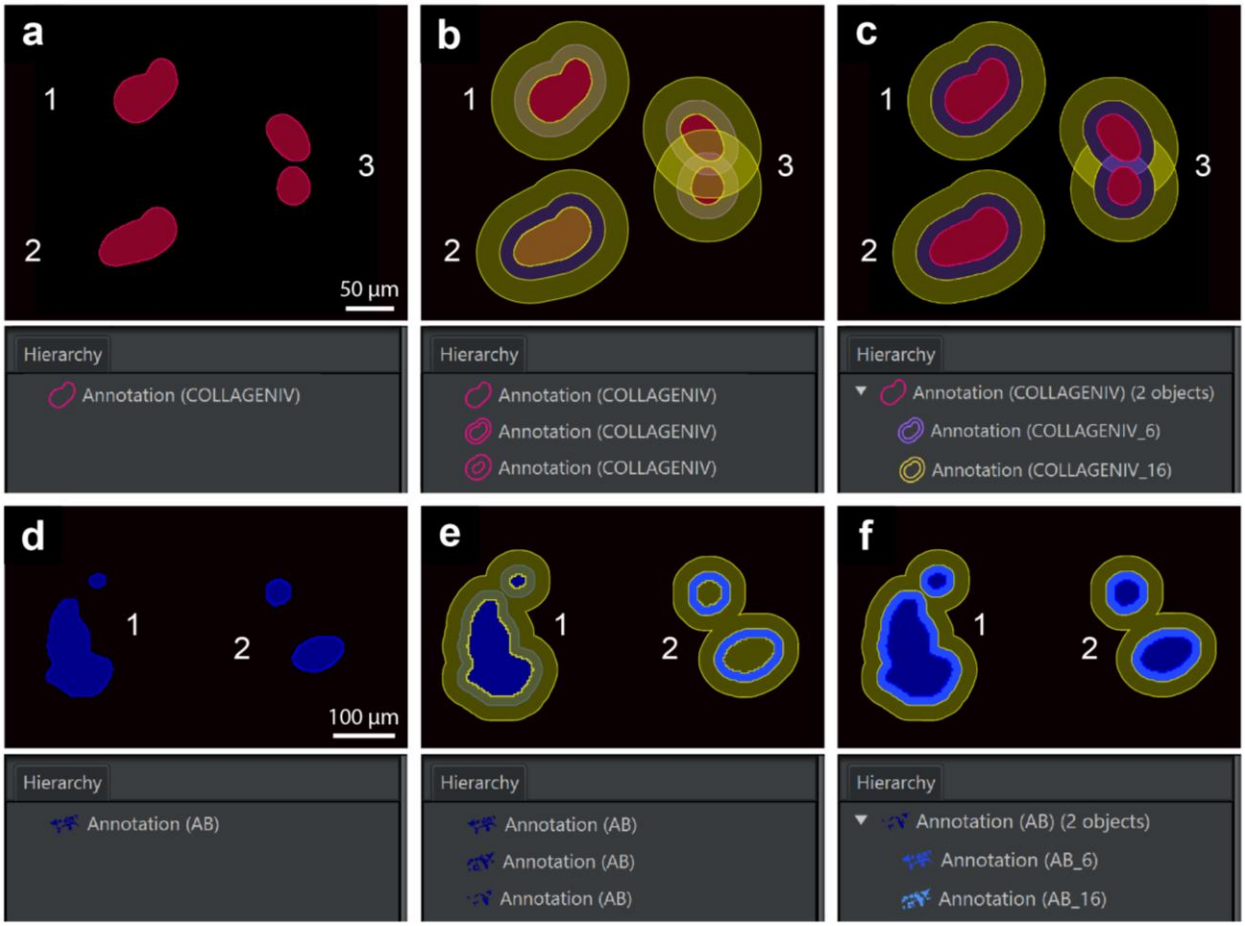

a
1
2
3
50 µm
Hierarchy
Annotation (COLLAGENIV)
b
1
2
3
Hierarchy
Annotation (COLLAGENIV)
Annotation (COLLAGENIV)
Annotation (COLLAGENIV)
c
1
2
3
Hierarchy
Annotation (COLLAGENIV) (2 objects)
Annotation (COLLAGENIV_6)
Annotation (COLLAGENIV_16)
d
1
2
100 µm
Hierarchy
Annotation (AB)
e
1
2
Hierarchy
Annotation (AB)
Annotation (AB)
Annotation (AB)
f
1
2
Hierarchy
Annotation (AB) (2 objects)
Annotation (AB_6)
Annotation (AB_16)

Figure 3

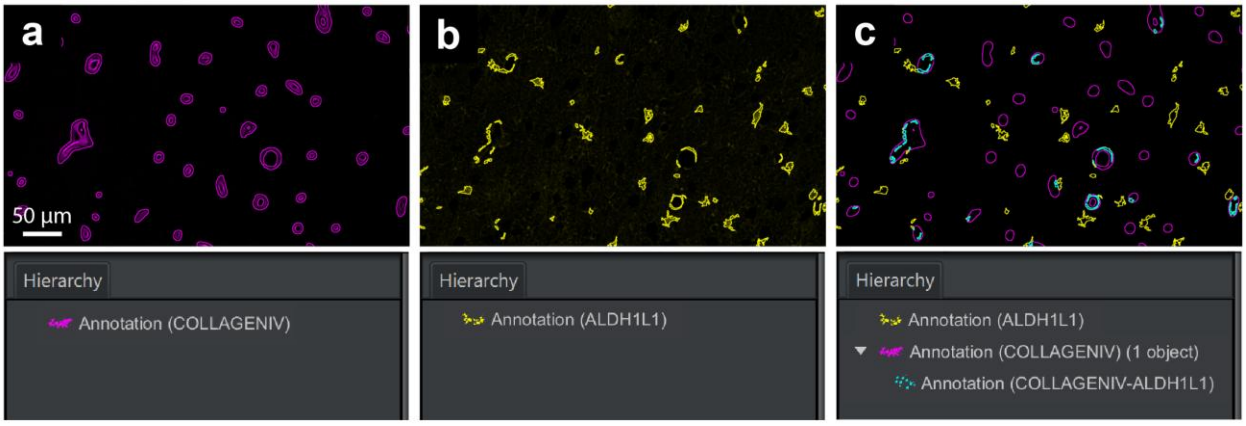

a
50 µm
b
c
Hierarchy
Annotation (COLLAGENIV)
Hierarchy
Annotation (ALDH1L1)
Hierarchy
Annotation (ALDH1L1)
Annotation (COLLAGENIV) (1 object)
Annotation (COLLAGENIV-ALDH1L1)

Figure 4

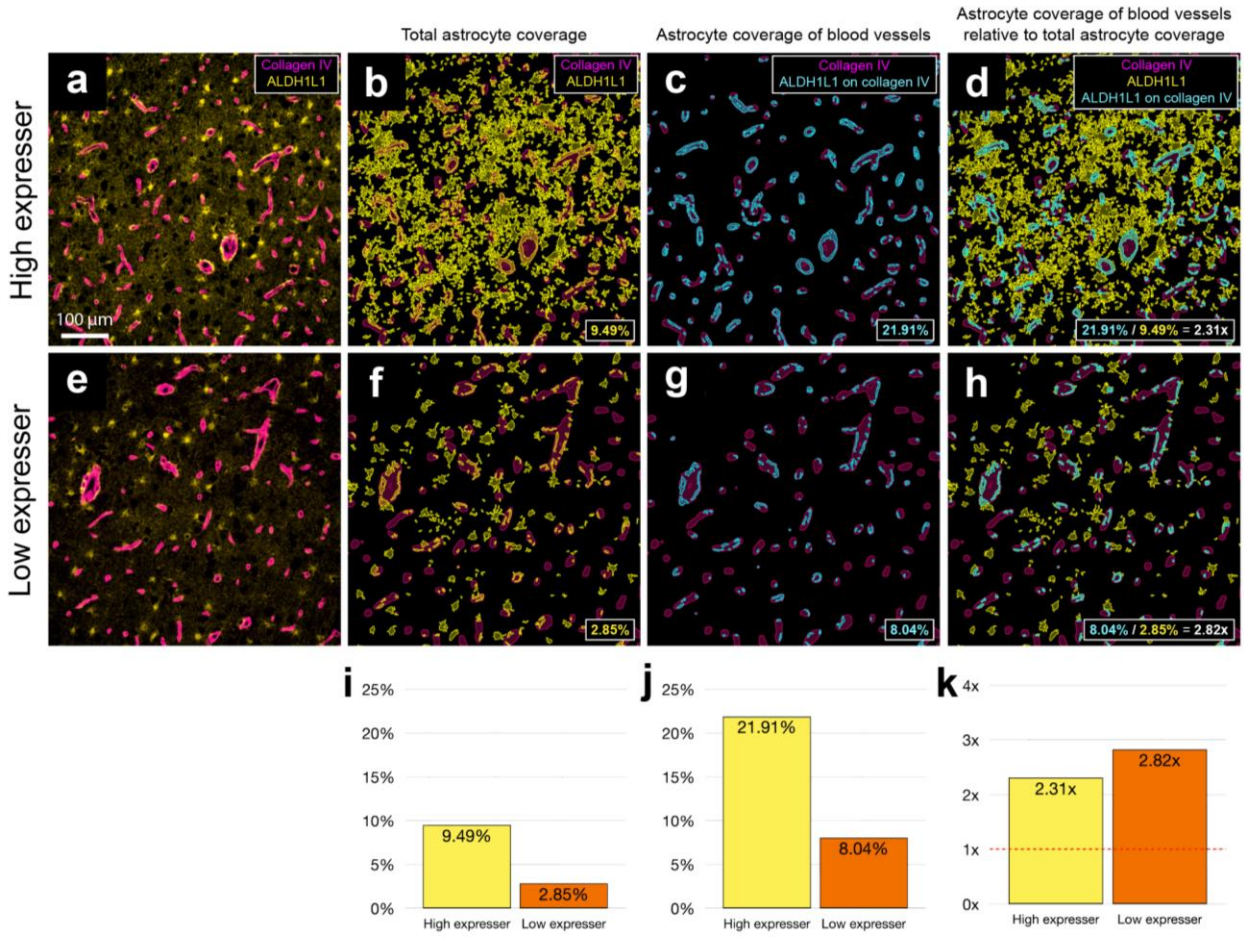

Total astrocyte coverage
Astrocyte coverage of blood vessels
Astrocyte coverage of blood vessels relative to total astrocyte coverage
High expresser
Low expresser
a
b
c
d
e
f
g
h
Collagen IV
ALDH1L1
ALDH1L1 on collagen IV
100 µm
9.49%
21.91%
21.91% / 9.49% = 2.31x
2.85%
8.04%
8.04% / 2.85% = 2.82x
i
j
k
25%
20%
15%
10%
5%
0%
4x
3x
2x
1x
0x
2.31x
2.82x
High expresser
Low expresser

Figure 5

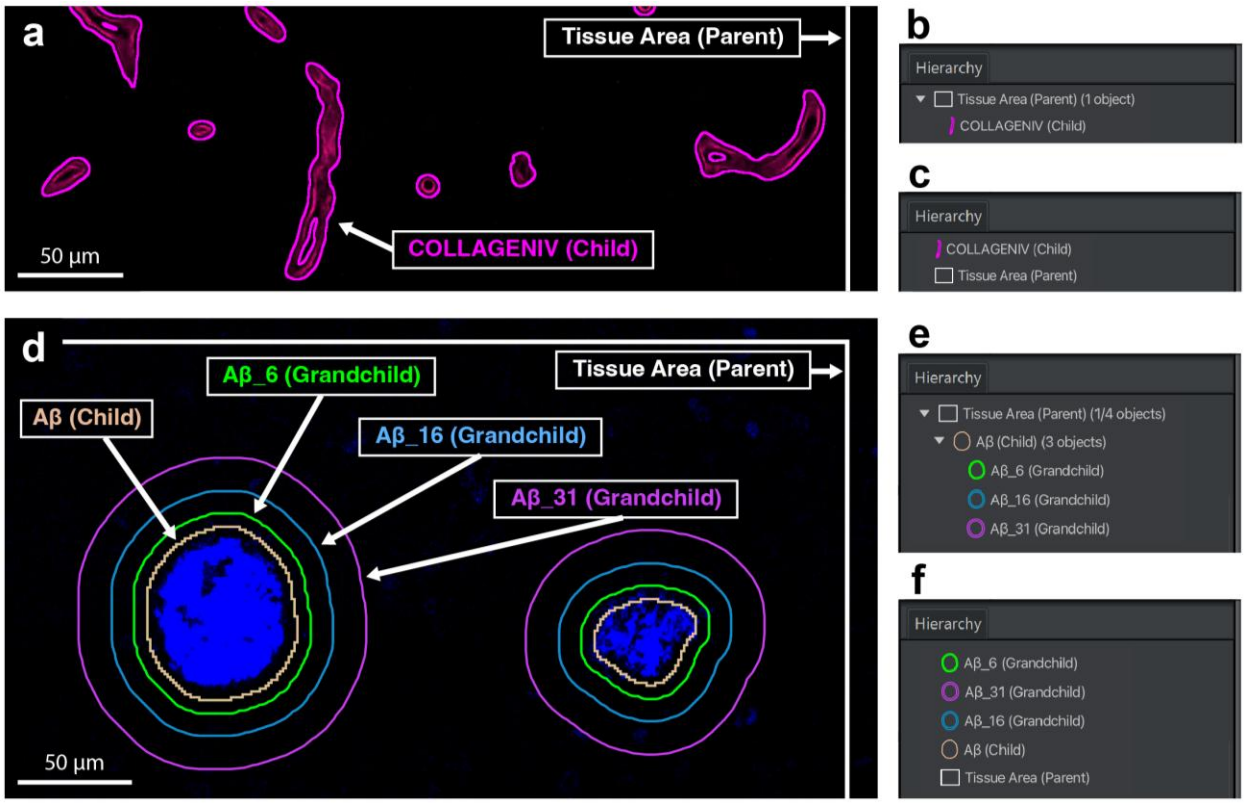

a
Tissue Area (Parent)
COLLAGENIV (Child)
50 µm
b
Hierarchy
Tissue Area (Parent) (1 object)
COLLAGENIV (Child)
c
Hierarchy
COLLAGENIV (Child)
Tissue Area (Parent)
d
Aβ_6 (Grandchild)
Tissue Area (Parent)
Aβ (Child)
Aβ_16 (Grandchild)
Aβ_31 (Grandchild)
50 µm
e
Hierarchy
Tissue Area (Parent) (1/4 objects)
Aβ (Child) (3 objects)
Aβ_6 (Grandchild)
Aβ_16 (Grandchild)
Aβ_31 (Grandchild)
f
Hierarchy
Aβ_6 (Grandchild)
Aβ_31 (Grandchild)
Aβ_16 (Grandchild)
Aβ (Child)
Tissue Area (Parent)

Figure 6

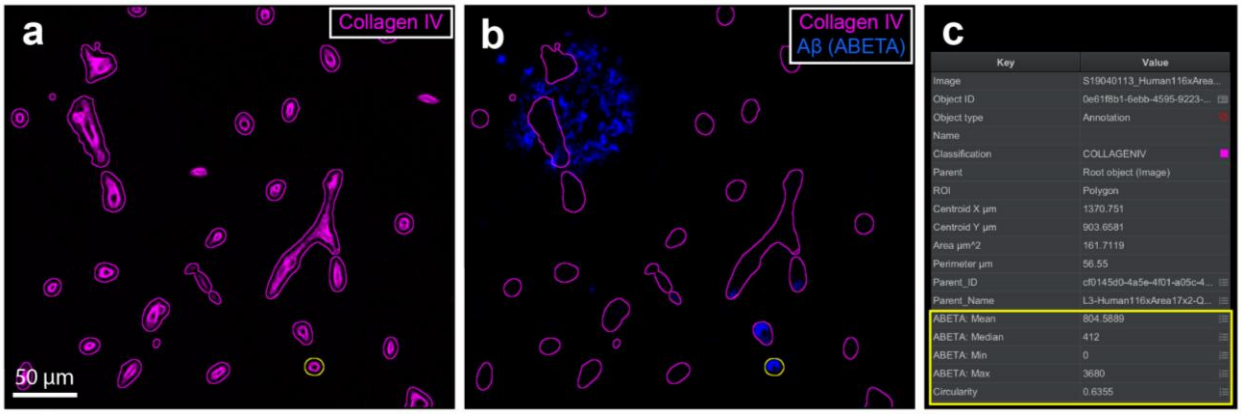
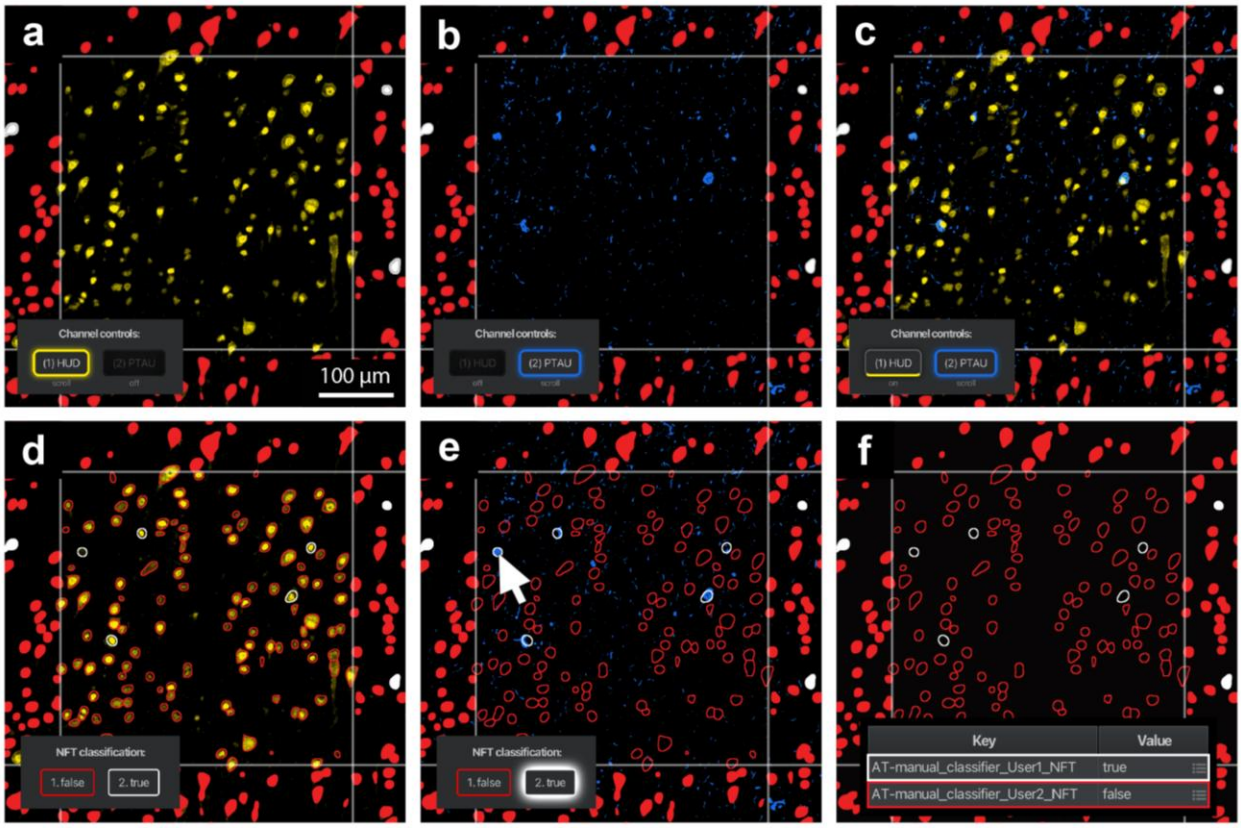

a
Collagen IV
50 µm
b
Collagen IV
Aβ (ABETA)
c
Key
Value
Image
S19040113_Human116xArea...
Object ID
0e61f8b1-6ebb-4595-9223-...
Object type
Annotation
Name
Classification
COLLAGENIV
Parent
Root object (Image)
ROI
Polygon
Centroid X µm
1370.751
Centroid Y µm
903.6581
Area µm^2
161.7119
Perimeter µm
56.55
Parent_ID
cf0145d0-4a5e-4f01-a05c-4...
Parent_Name
L3-Human116xArea17x2-Q...
ABETA: Mean
804.5889
ABETA: Median
412
ABETA: Min
0
ABETA: Max
3680
Circularity
0.6355

Figure 7


a
Channel controls:
(1) HUD
(2) PTAU
100 µm
b
Channel controls:
(1) HUD
(2) PTAU
c
Channel controls:
(1) HUD
(2) PTAU
d
NFT classification:
1. false
2. true
e
NFT classification:
1. false
2. true
f
Key
Value
AT-manual_classifier_User1_NFT
true
AT-manual_classifier_User2_NFT
false

Supplementary Files

This is a list of supplementary files associated with this preprint. Click to download.

- SupplementaryMaterials.pdf